Visualizing Volcanic Clouds in the Atmosphere and their Impact on Air Traffic

Tobias Günther Maik Schulze Anke Friederici Holger Theisel
University of Magdeburg

Abstract

Volcanic eruptions are not only hazardous in the direct vicinity of a volcano, but also affect the climate and air travel at larger distance. In this paper, we present our results on the 2014 IEEE Scientific Visualization Contest, which centers around the fusion of multiple satellite data modalities to reconstruct and assess the movement of volcanic ash and sulfate aerosol emissions. In particular, we shed light on the Grímsvötn, Puyehue-Cordón Caulle and Nabro eruptions in 2011. We study the agreement of the complementary satellite data, reconstruct sulfate aerosol and volcanic ash clouds, visualize endangered flight routes, minimize occlusion in particle trajectory visualizations and finally focus on the main pathways of Nabro's sulfate aerosol into the stratosphere.

1 Introduction

In this paper, we present our findings on the aftermath of three volcanic eruptions as a contribution to the 2014 IEEE Scientific Visualization Contest. Our analysis is based on the fusion of different atmospheric data modalities in order to assess the plume development after three volcanic eruptions that occurred in a short span of about three weeks. These are the volcanoes Grímsvötn in Iceland (eruption on May 21st, 2011), Puyehue-Cordón Caulle in Chile (eruption on June 4th, 2011) and Nabro in Eritrea (eruption on June 13th, 2011). All three caused major air traffic restrictions. The Nabro eruption spurred a series of studies and a dispute among climate scientists on the pathway of Nabro's sulfate aerosol into the stratosphere [BRR*12, VTF*13, BRR*13, FKN*14]. One goal of the contest was to use insightful visualizations to contribute to this atmospheric research problem.

The contest was hosted by RWTH Aachen University and the data and tasks were provided by the Simulation Laboratory Climate Science at the Jülich Supercomputing Centre and the Institute of Energy and Climate Research, both resided at the Research Center Jülich, Germany. An overview of the provided data is shown in Fig 1. More specifically, the contest data comprises discrete, time-dependent, mutually exclusive vertical ash, sulfate aerosol, ice and clear air detections, all captured by the Michelson Interferometer for Passive Atmospheric Sounding (MIPAS) [GHSR14], which is aboard ESA's Envisat satellite. The measurements sum up to roughly 1.29 million points (42 MB of memory in total). Furthermore, altitude-integrated volcanic ash and SO_2 concentration are measured using index methods by the Atmospheric Infrared Sounder (AIRS) [CPA*06, HGM14] aboard NASA's Aqua satellite. The measurements are taken on thin polygon strips along the satellite's ground track, which results in 12.8 GB of memory for the entire time sequence. The measurements are taken along roughly sinusoidal ground tracks that leave measurement gaps at low and mid-latitudes. Trajectories of 61,324 particles are seeded at MIPAS detections of volcanic ash or sulfate aerosol and are calculated by the Chemical Lagrangian Model of the Stratosphere (CLaMS) [MKG*02, KGM*07, KGG*10] that has recently been extended to the troposphere [PKM*12].

The trajectories and their associated scalars, e.g., temperature and pressure, sum up to 1.04 GB. The CLaMS simulation is based on the ERA-Interim [DUS*11] meteorological reanalysis, which was also source of the tropopause altitude data set.

David Feng – *Allen Brain Institute*
Bernd Hentschel – *Virtual Reality Group, RWTH Aachen University, JARA – High Performance Computing*

Introduction

Each year, the IEEE Scientific Visualization Contest presents researchers from the visualization community an opportunity to transfer the latest developments in visual data analysis to a challenging, real-world application scenario. Details on this year's event and past contests are available via http://sciviscontest.ieeevis.org.

The Contest Problem

For 2014, the contest targeted data from atmospheric research which captures volcanic eruptions and their atmospheric aftermath. The data comprised recordings from two different satellite instruments, namely the Michelson Interferometer for Passive Atmospheric Sounding (MIPAS) and the Atmospheric Infrared Sounder (AIRS), and simulation results generated with the Chemical Lagrangian Model of the Stratosphere (CLaMS). The contest challenged participants to create a comprehensive visualization of the given data which should help domain scientists to better understand the consequences of volcanic events for atmosphere and climate. The integration of all data modalities allows researchers to gain new insights into the dispersion and transport pathways of volcanic aerosol.

The data covered a particularly interesting period of time from mid-May to the end of July 2011; within three weeks three volcanoes erupted in three different climate zones. The series started on May, 21st with the eruption of the Icelandic Grímsvötn volcano. This eruption emitted significant amounts of sulfur dioxide as well as ash particles into the Arctic atmosphere. On June, 4th, the Chilean Puyehue-Cordón Caulle injected several million tons of ash into the southern hemisphere mid-latitudes. The eruption reached the lower stratosphere and the ash was transported by the jet stream around the globe. Several hundred flights in South America, Australia, and New Zealand had to be canceled. The eruption of the Eritrean Nabro volcano started on June, 13th. This eruption in the tropics is most notably known for the large amounts of sulfur dioxide that entered the upper troposphere and lower stratosphere.

The contest consisted of five tasks, ranging from the development of rather straightforward browsing capabilities to a discussion of a yet unresolved research question related to the June 2011 eruption of Nabro. For more information, we refer to the contest web site at http://sciviscontest.ieeevis.org/2014/.

Evaluation

We received six submissions. A jury of three domain scientists (Sabine Grießbach, Lars Hoffmann, and Marc von Hobe) and three visualization researchers (Theresa-Marie Rhyne, Christoph Garth, and Bernd Hentschel) carefully reviewed all entries. Since the main goal of the visualization contest is to promote the transfer of cutting-edge visualization research to specific application domains, the domain experts' assessment was favored with 75% over 25% for the visualization reviews. Hence, successful entries should first and foremost provide an insightful visualization that actually helps atmospheric researchers.

The jury selected the entry *"Visualizing the Aftermath of Volcanic Eruptions"* by T. Günther, M. Schulze, A. Friederici, and H. Theisel, all of whom are with the University of Magdeburg as the overall contest winner. The present article is an extended discussion of their results. However, this year's decision has been extremely close, in fact so much so that the jury decided to award an "Honorable Mention" to the entry *"SPatial Atmospheric Cloud Explorer – SPACE"* by J. Xie, F. Sauer, H. Schroots, C. Wang, S. Wang, and K. L. Ma, University of California at Davis.

Acknowledgements

The data set for this contest has been kindly provided by the Simulation Laboratory Climate Science at the Jülich Supercomputing Centre and the Institute of Energy and Climate Research, both at Research Center Jülich, Germany within JARA – High Performance Computing. We would like to thank Sabine Grießbach, Lars Hoffman, Marc von Hobe, Christoph Garth, Theresa-Marie Rhyne, Tatyana Povalyaeva, and Amit Chourasia for their continued support throughout the entire contest.

The tropopause is the boundary between troposphere and stratosphere. Its altitudes (potentially two layers) are provided on a uniform grid for 320 time steps, which totals 477 MB.

2 Data Preprocessing

Taken by the near-polar sun-synchronous satellite orbit, the MIPAS and AIRS measurements are arranged along roughly sinusoidal ground tracks that cover the globe, see again Fig. 1. Since both satellites orbit the globe about 14 times a day and measure only within a small band, the concentration indices and detection measurements are quite sparsely represented in both space and time. To fill in the blank areas in AIRS, we interpolate values from the two closest time steps and inspect the temporal distance in Fig. 2. As indicated in Fig. 2(b) by red arrows, this interpolation method entails small reconstruction artifacts, because in its essence, it simply blends between adjacent time steps. To reduce noise, we convolve the interpolated AIRS measurements with a Gaussian kernel. For faster access on the GPU, we resample the AIRS data onto a uniform grid with 1000×500 cells at 600 time steps, which totals for both volcanic ash and SO_2 indices 2×1.11 GB.

3 Data Analysis

The data needed at runtime is within gigascale range, making it comfortable to process it on a single machine. Thus, we keep all AIRS, MIPAS, CLaMS

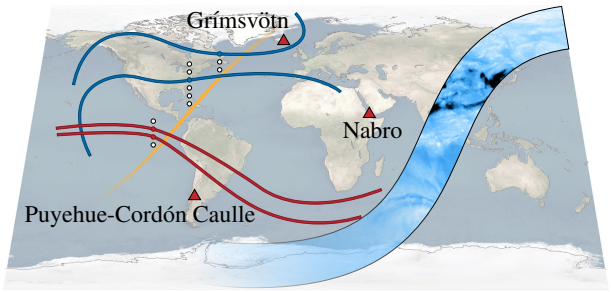

Figure 1: Overview of the principal data. The locations of volcanoes are depicted by (▲) glyphs. MIPAS detects sulfate aerosol and volcanic ash vertically along the orange ground track, whereas AIRS uses index methods to measure altitude-integrated SO_2 and ash concentration, shown in the wider blue ground track. CLaMS trajectories are seeded at MIPAS detections of volcanic ash (●) and sulfate aerosol (●).

and the tropopause data in RAM and selectively stream the data of the current time slice to the GPU for display. On a general note, all data modalities have already been registered and are defined in geographical latitude and longitude coordinates with an optional altitude dimension. Thus, in the remainder of the paper, we measure distances on the globe by geodesics in spherical coordinates. First, we integrate the data into a comprehensive and interactive overview visualization, as described in the following.

3.1 Overview and Data Browsing

An overview of the data is shown in Fig. 3. Here, all MIPAS, AIRS and CLaMS data can be interactively explored, transfer functions adjusted and data attributes visualized, such as altitude, pressure or temperature. The user can switch between a planar 3D view with altitude mapped to height and a spherical view, which both have their individual strengths and weaknesses, i.e., distortion at the poles or occlusion of the back-facing hemisphere. To avoid clutter in the exploration process, we allow the user to specify a time frame that hides CLaMS and MIPAS data outside the time range. Typically, the time frame is set to a few hours or days. Thereby, the center of the frame determines the sampling time for the display of continuous data, such as the resampled AIRS measurements. In Fig. 3, June 18th is currently selected as center time, with trajectories shown for a time frame of 3 days. The CLaMS trajectories are only shown for the Southern Hemisphere and are color-coded by altitude. The MIPAS detections are depicted as colored dots, with yellow encoding a sulfate aerosol and red an ash detection. MIPAS detections of air and ice are hidden in this image. The map in the background color-codes resampled AIRS values, showing an SO_2 cloud emitted from the Nabro volcano.

Combining individual satellite data into one visualization also allows to locate and judge areas at which the modalities disagree. MIPAS and AIRS are known to exhibit a different sensitivity to aerosols. Consequentially, it is expected that both satellites will reach different answers in areas of low concentration. In Fig. 4, we map at each MIPAS ash and sulfate aerosol detection the corresponding AIRS concentration indices to color. In addition, we create histograms of AIRS indices sampled at MIPAS detections. The ash index histogram in Fig. 4(a) (computed for the entire

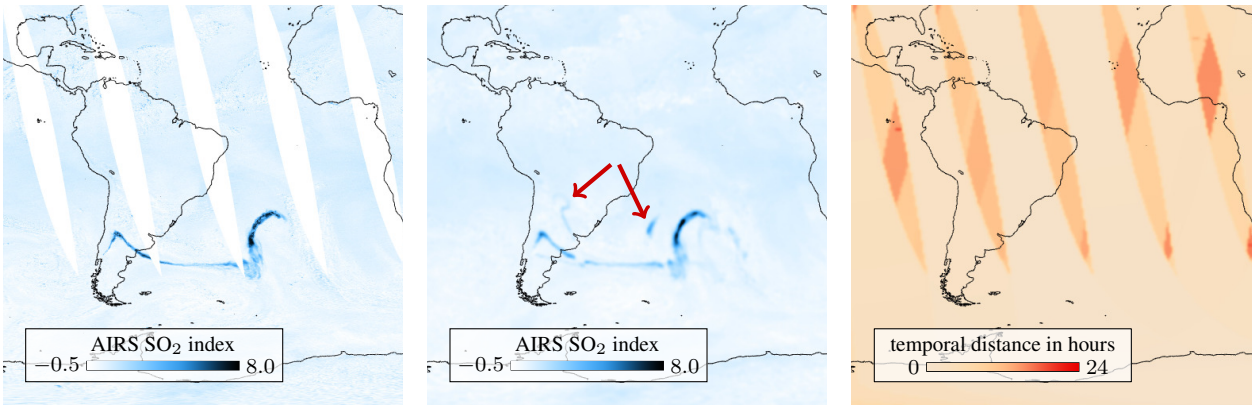

(a) Original AIRS data (single time slice).

(b) Resampled AIRS data (single time slice).

(c) Temporal distance to the closest measurement.

Figure 2: Preprocessing results of AIRS data. The first two images show the SO_2 index on June 6th, measured shortly after the eruption of the Puyehue-Cordón Caulle volcano. A high SO_2 index correspond to a high concentration. The original data (a) has measurement gaps, which we fill in a resampling step (b). Note that reconstruction artifacts may appear, as we interpolate values from nearby time slices. The temporal distance to the closest measurement is shown in (c).

sequence) shows that the majority of the MIPAS detections has an ash index < 4. For sulfate aerosol in Fig. 4(b), however, many detections are in range of a particularly low AIRS SO_2 index, especially detections that originated from the earlier Grímsvötn eruption. This is because SO_2 oxidizes to sulfate aerosol within a few days, whereas sulfate aerosol remains for weeks. When all SO_2 is gone, only sulfate aerosol remains. As visible on the map, most of the sulfate aerosol detections occur in the North.

3.2 Linking Measurements to Volcanoes

The volcanic eruptions happened over a span of three weeks. While Puyehue-Cordón Caulle seems easily separable from the others as it is on the Southern Hemisphere, Grímsvötn and Nabro are close enough for their aerosol clouds to mix. In order to identify the volcano that emitted the ash or sulfate aerosol that was found by a particular MIPAS detection, we trace the CLaMS trajectories, which were seeded at those MIPAS detections, backward in time. For each vertex of a trajectory, we compute the distance to all volcanoes and consider the closest a potential source, if the volcano was passed while it was active. From there on, a CLaMS trajectory and its MIPAS detection (the seed point) are associated with the closest volcano if the minimal distance is below a user-defined threshold, which we empirically set to about 250 km. This distance is a rather conservative choice, which accomodates for possible deviations in the backward integration of the CLaMS trajectories, because generally, tropospheric trajectories are most reliable up to five days. Note that the CLaMS data that the classification is based upon ends one month before the end of MIPAS detections. Consequentially, MIPAS detections in the remaining month are without classification. (Even if CLaMS data was available, the temporal distance to the eruptions would be too large for reliable classification.)

Since CLaMS trajectories in the North start at the time of the Nabro eruption (June 12th), they cannot be used to determine whether a MIPAS detection belonged to the earlier Grímsvötn eruption (May 21st). For this reason, we need a special handling to detect the residuals of the Grímsvötn cloud. Observing the classification results of the aforementioned CLaMS-based association heuristic, we eventually end up with a number of MIPAS aerosol detections (80.5 %) that cannot be associated with a volcano. Among these unclassified MIPAS detections, we use the AIRS measurements to associate MIPAS and CLaMS detections with the Grímsvötn volcano by using a suitable threshold on the volcanic ash index. (We found the sulfate aerosol concentrations to be insufficiently descriptive.) The histogram in Fig. 4 suggests that MIPAS detects volcanic ash in regions with an ash index < 4,

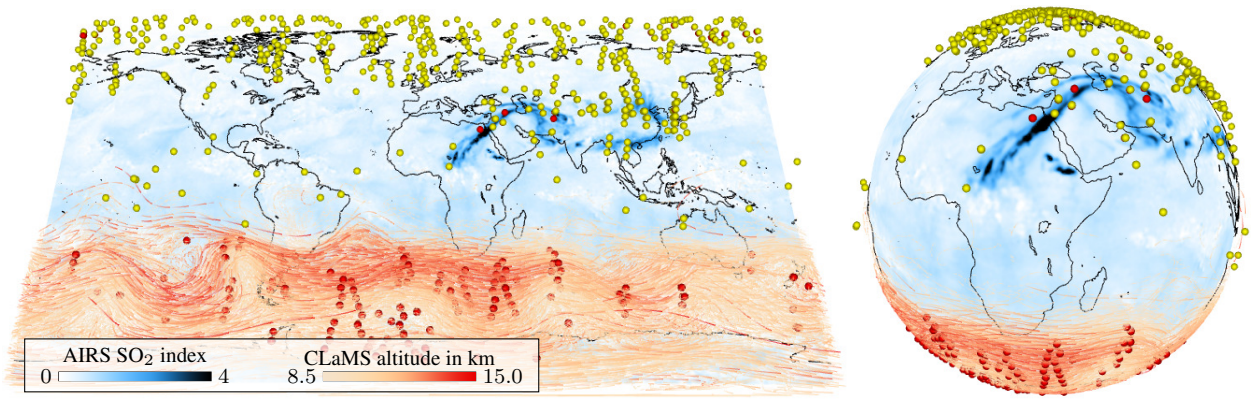

Figure 3: Here, the main input data (MIPAS, AIRS and CLaMS) is combined in an interactive visualization that allows to slice in time, apply transfer functions, and map varying data attributes (pressure, temperature, etc.) to the trajectories. The user can instantly switch between a planar 3D view with altitude mapped to height and a spherical view.

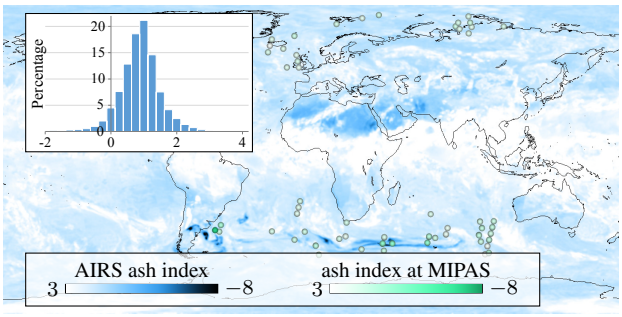

(a) AIRS Ash index on June 8th, shortly after the Puyehue-Cordón Caulle eruption and a histogram of sampled AIRS ash indices at MIPAS ash detections.

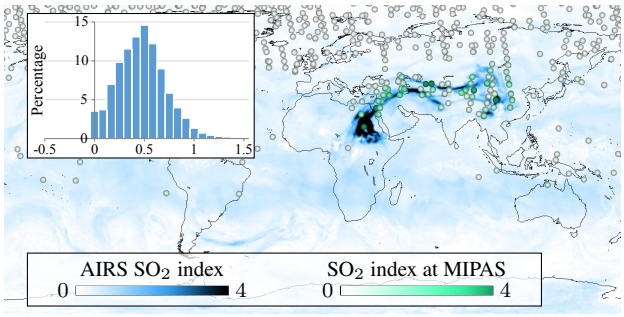

(b) AIRS SO_2 index on June 16th, shortly after the Nabro eruption and a histogram of sampled AIRS SO_2 indices at MIPAS sulfate aerosol detections.

Figure 4: Visualization of AIRS concentration indices at the MIPAS detections in a time frame of 3 days. A negative ash index and a positive SO_2 index correspond to high concentration.

which we use as a conservative threshold. Later, transparency is used to fade out areas with an ash index > 0, but during cloud reconstruction it is advisable to have more trajectories that carry potentially varying ash concentrations. If these ash detections are north of $55°$ N and not yet associated with a volcano they are likely to belong to Grímsvötn, which equals to roughly $1.0\,\%$ of all MIPAS ash or sulfate aerosol detections (of the entire time sequence). A classification of the CLaMS trajectories to the potential source volcanoes is shown in Fig. 5.

3.3 Ash Cloud Reconstruction

We move on to the reconstruction of ash clouds, which we discretize into a uniform 3D scalar field with $1000 \times 500 \times 32$ voxels. AIRS measurements are altitude-integrated, which we distribute along altitude using CLaMS and MIPAS. For this, we create at every AIRS measurement a probability distribution $f(z)$ of the ash concentration along the altitude z. Thereby, we aim for two things. First, MIPAS detections should be transported along CLaMS trajectories, as these are the actual pathways of the ash. Second, $f(z)$ should correspond to the density of ash-laden CLaMS trajectories, as high density has a higher probablity to indicate the ash transport path. For the first, we start at the MIPAS seed vertices and iterate the trajectories in both directions. In case a MIPAS detection is found near a vertex (distance $< 128\,\text{km}$, altitude difference $< 5\,\text{km}$ and time difference < 1.5 hours), we assign the detection value (i.e., $\text{ash} = 1$ or $\text{clear air} = 0$) to the following vertices until another detection is found or the trajectory ends. Afterwards, we diffuse the assigned values, assuming that the de-

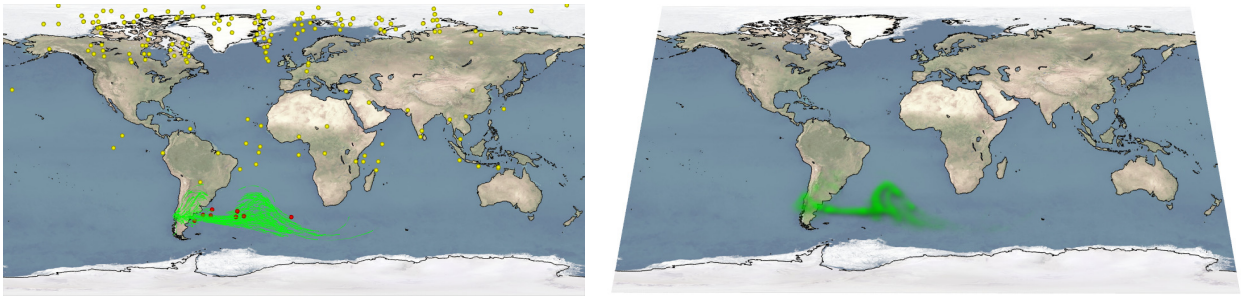

(a) June 6th, two days after Puyehue-Cordón Caulle eruption (36 hour time frame).

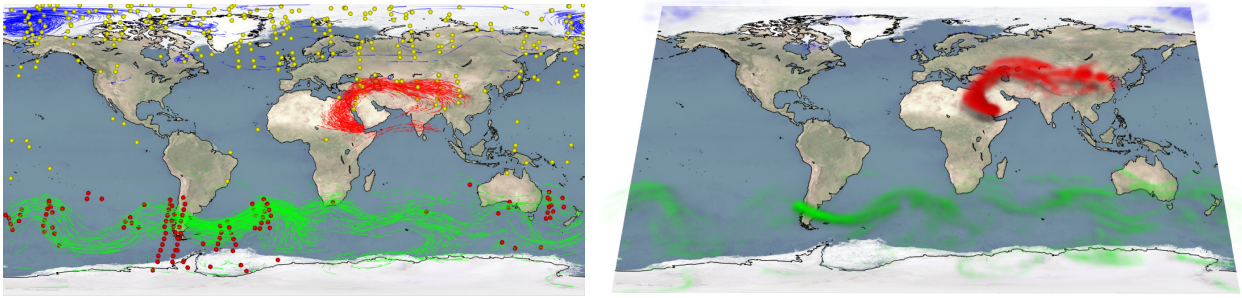

(b) June 16th, three days after Nabro eruption (36 hour time frame).

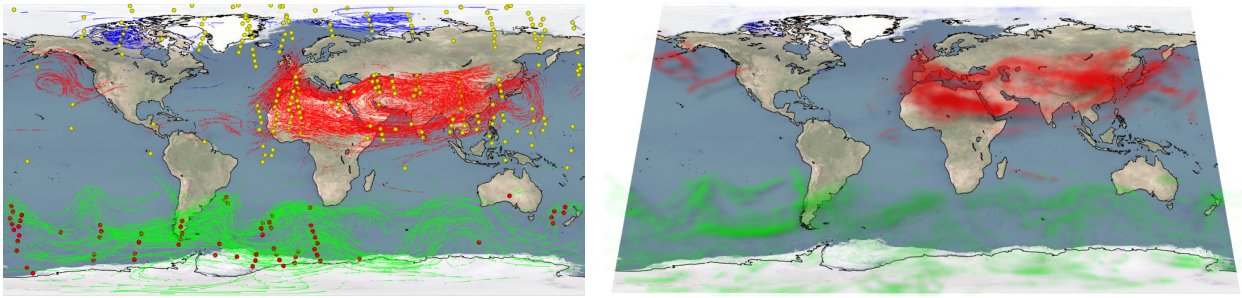

(c) June 28th, fifteen days after Nabro eruption (36 hour time frame).

Figure 5: On the left, the classification of CLaMS trajectories to the three volcanoes Grímsvötn (•), Puyehue-Cordón Caulle (•) and Nabro (•) is shown. For reference, MIPAS detections are shown by points in yellow (sulfate aerosol) and red (ash). On the right, the resulting 3D sulfate aerosol cloud reconstructions are shown.

tected ash is transported. For the second, we rasterize the detection values of all CLaMS trajectories into a 3D scalar field, using additive blending. We use one scalar field for each volcano and another one for unclassified trajectories in order to discriminate them. Thereby, we obtain an ash detection frequency h_v at every voxel v. To ensure independence of the grid resolution, the ash concentration $c(z)$ of a voxel is obtained by dividing h_v by the voxel volume. The probability distribution $f(z)$ of the ash concentration follows from normalizing the ash concentration $c(z)$ such that $\int f(z)\mathrm{d}z = 1$. Using the 2D AIRS ash index A_{2D}, we reconstruct our 3D ash index $A_{\mathrm{3D}}(z)$:

$$A_{\mathrm{3D}}(z) = A_{\mathrm{2D}}\, f(z) - \gamma\, c(z)\,.$$

Setting $\gamma = 0$ distributes the AIRS ash index along the altitude axis according to the probability distribution $f(z)$, thereby trusting only AIRS. But since MIPAS is known to be more sensitive than AIRS, we introduce a γ-parameter that allows the MIPAS-guided ash concentration $c(z)$ to overrule the AIRS decision. In its essence, γ balances the trust between AIRS and MIPAS. Results of reconstructed ash clouds for a varying γ are shown in Fig. 6. There, the clouds of the volcanoes Grímsvötn (•), Puyehue-Cordón Caulle (•) and Nabro (•) are color-coded, whereas white clouds

denote ash that our aforementioned CLaMS- based heuristic did not associate with a volcano. To provide a sense of depth, all clouds are shaded by Fourier opacity mapping [JB10], using a 512×512 shadow map. The MIPAS ash detections are color-coded in red for reference, showing that for $\gamma = 2$ we are able to reconstruct the clouds at those sensitive detections, which was not possible with AIRS alone, i.e., $\gamma = 0$. The accompanying video contains animations of the reconstructed ash clouds.

Following the same idea, sulfate aerosol clouds are visualized in Fig. 5 by GPU-based ray casting. Note that for the sulfate aerosol reconstruction on the Southern Hemisphere, there were no MIPAS sulfate aerosol detections south of 20° S. Thus, there, only CLaMS and AIRS could be used, i.e., we assume that all CLaMS trajectories carry the same amount of sulfate aerosol and we redistribute the altitude-integrated 2D AIRS SO_2 index, simply based on the observed CLaMS density along the altitude axis.

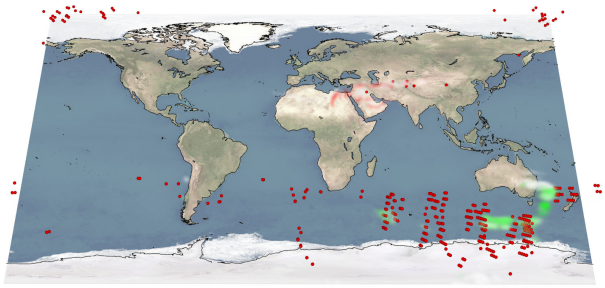

(a) $\gamma = 0$, poor reconstruction.

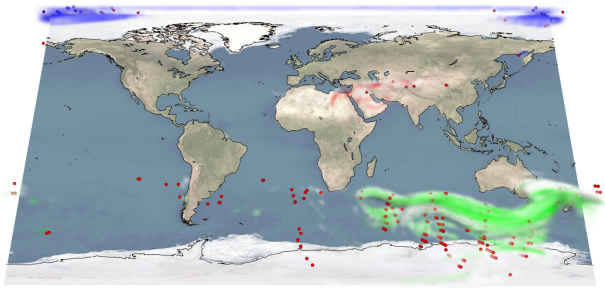

(b) $\gamma = 1$, main body of cloud reconstructed.

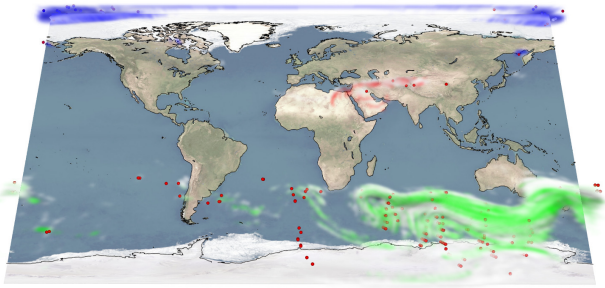

(c) $\gamma = 2$, reconstructed finer details as well.

Figure 6: Ash cloud reconstruction with an ash index< 0 for varying γ on June 21st. Clouds are color-coded by their source volcano (see text). MIPAS volcanic ash detections are shown as a reference.

3.4 Dangerous Flight Routes

Using open air traffic data[1], we generate 73,098 exemplary airplane routes, which are visualized in Fig. 7. The route computation is based on geodesics and models altitude parametrically for climb, cruise and descent phases. In this context, the visualization also shows the reconstructed 3D ash clouds for $\gamma = 2$ in a 36 hours time frame. As before, MIPAS ash detections are color-coded in red for reference and the clouds of the volcanoes Grímsvötn (●), Puyehue-Cordón Caulle (●) and Nabro (●) are color-coded, whereas white clouds denote ash that our CLaMS-based heuristic did not associate with a vol-

[1] www.OpenFlights.org

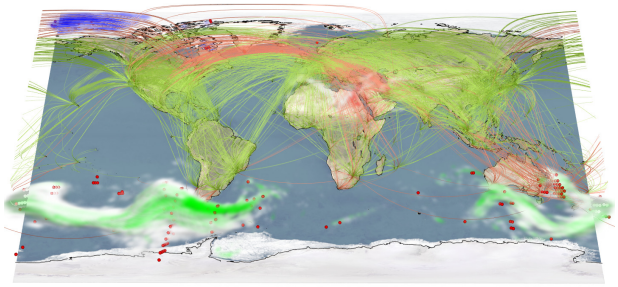

(a) Airplane routes on June 15th.

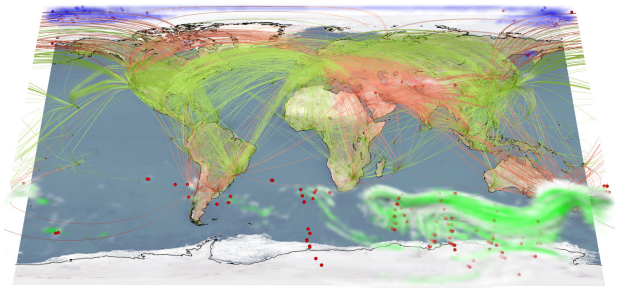

(b) Airplane routes on June 21st.

Figure 7: Visualization of air traffic routes that were affected by volcanic ash clouds. The clouds are color-coded by their source volcano (see text). Green flight routes are safe and red one are considered dangerous.

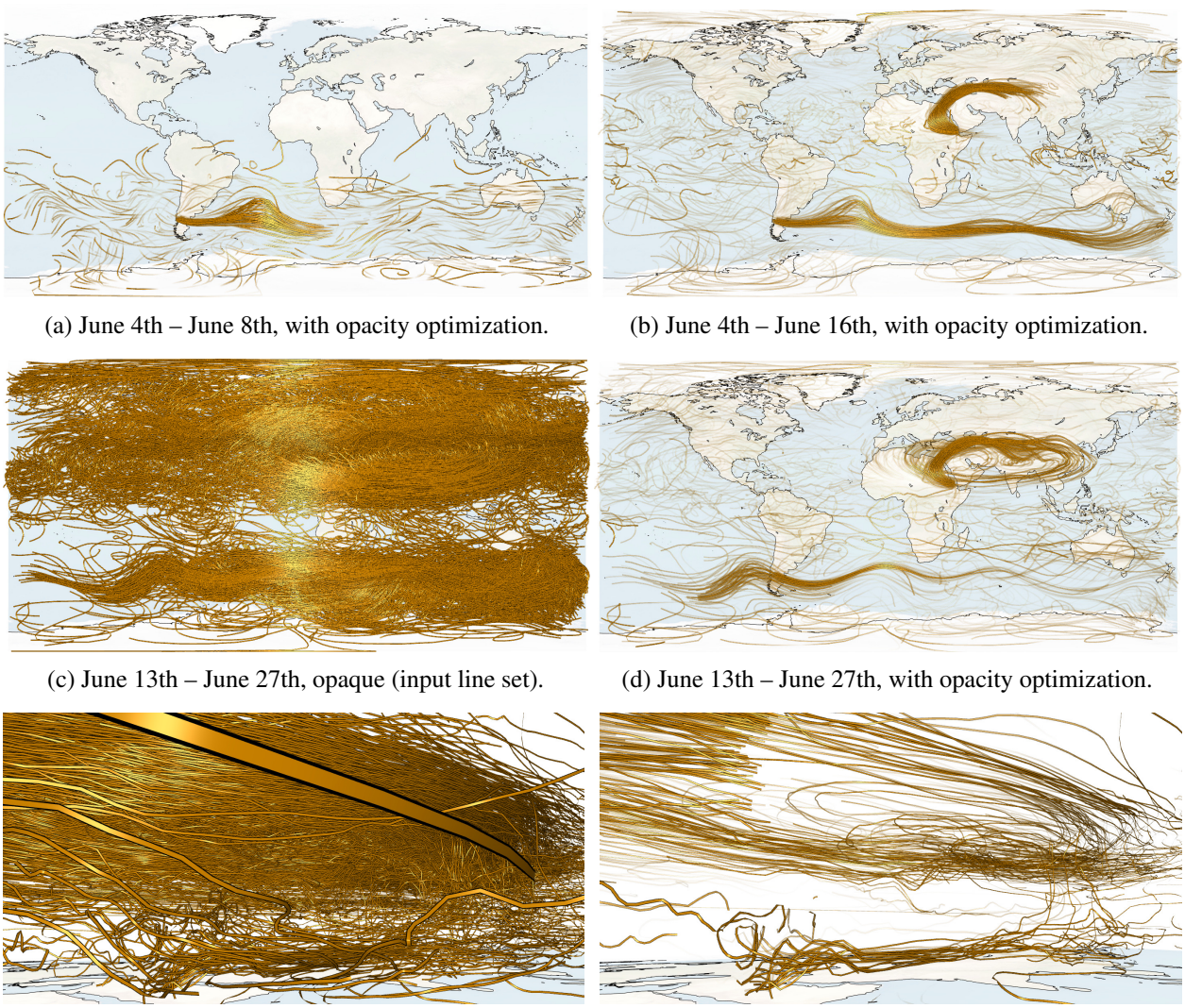

(a) June 4th – June 8th, with opacity optimization.

(b) June 4th – June 16th, with opacity optimization.

(c) June 13th – June 27th, opaque (input line set).

(d) June 13th – June 27th, with opacity optimization.

(e) June 21st – July 5th, opaque (input line set).

(f) June 21st – July 5th, with opacity optimization.

Figure 8: CLaMS trajectories occlude each other rather strongly. For this reason, we use hierarchical opacity optimization [GRT14], which computes an optimal assignment of line opacities so that the view is cleared on CLaMS trajectories with high sulfate aerosol concentration.

cano. Flight routes that pass a region with a negative ash index $A_{3D} < 0$ are color-coded in red, showing routes that should conceptually be canceled, as they would enter a potentially dangerous flight corridor. Safe airplane routes are depicted in green. The animation in the accompanying video shows when airports in Chile, Argentina, South Africa, Southern Australia and New Zealand were worst affected by the Puyehue-Cordón Caulle ash cloud.

3.5 Visualization of CLaMS Trajectories

The CLaMS trajectories are essential for the linking of MIPAS measurements to the volcanic events. Their sheer number, however, makes it difficult to visualize them properly, because of occlusions. Thus, in Fig. 8, we use hierarchical opacity optimization [GRT14], a recent visualization method that adjusts the opacity of lines in order to minimize the occlusion of important—here, sulfate aerosol-laden—lines. Thereby, we not only obtain a notion of the location of sulfate aerosol clouds, but also see unclassified transport paths as context. The lines are shaded as illuminated streamlines using the method of Zöckler et al. [ZSH96].

Figs. 8(a), (b) and (d) show CLaMS trajectories in different time frames. Thereby, Fig. 8(c) shows a

highly cluttered line set, which was used as input for the opacity optimization in (d). In Figs. 8(e) and (f), the view is cleared on Nabro CLaMS trajectories that have a high aerosol concentration and are affected by the Asian Monsoon circulation. For this 3D close-up, the camera is placed above Southern Africa looking north-northeast. Image 8(e) contains the cluttered input lines for which opacities are optimized in image 8(f). The lines near the ground visualize the path of sulfate aerosol that is carried within the Asian Monsoon circulation, which lifts up near the East China Sea. Note that the altitude of the lines is scaled considerably to make the altitude difference between lines in the stratosphere and troposphere apparent. Lines that start high above the volcano show aerosol that has been directly injected into the upper troposphere or even into the stratosphere, which is discussed next.

3.6 Aerosol in the Stratosphere

When volcanic aerosol enters the stratosphere it may remain there for months or years, where it absorbs solar radiation, leading to a cooling of the surface. At present, there is an ongoing dispute among climate scientists on how Nabro's aerosol entered the stratosphere. Two hypotheses exist that either argue for a direct injection of the volcanic emission (H1) [VTF*13, FKN*14] or the upward motion within the Asian Monsoon circulation (H2) [BRR*12, BRR*13]. The CLaMS trajectories that are relevant for the support or decline of these hypotheses and their intersections with the tropopause layer are shown in Fig. 9. In image 9(a) only the parts of the CLaMS trajectories are shown that are *above* the lower tropopause, i.e., the stratospheric trajectories. In the stratosphere, trajectories move in an anticyclonic, i.e., clock-wise, circulation over North Africa and Asia. The 2D close-up in Fig. 9(b) reveals areas in which CLaMS trajectories enter the stratosphere, which is above Eritrea, North India and the East China Sea.

There are a number of different indicators that suggest vertical transport, such as changes in pressure or potential temperature. An uplift in the troposphere leads to a drop in temperature, while in the stratosphere, temperature increases during uplift. The correlation of the scalar CLaMS attributes (potential temperature/vorticity, pressure and temperature) with the tropopause intersection is visualized in Fig. 10. Note that for the latter, lines that directly start above the

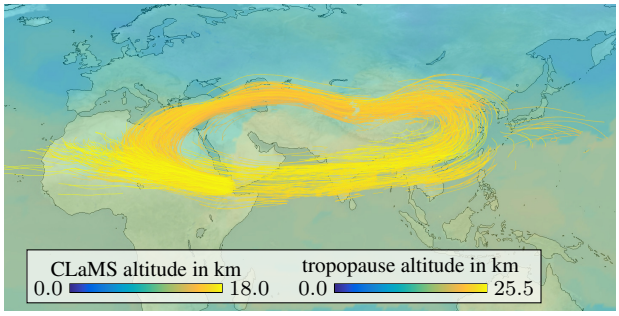

(a) A 3D top view on the lower tropopause and the CLaMS trajectories that are associated with the Nabro volcano.

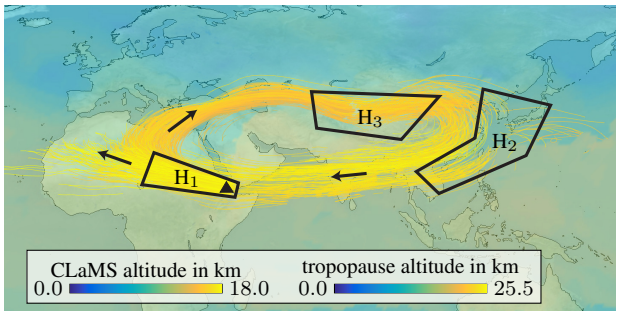

(b) A 2D close-up on stratospheric CLaMS trajectories.

Figure 9: CLaMS trajectories that are relevant for the Nabro volcano are shown together with the tropopause layer around June 21st, within a 3 days time frame. Both trajectories and tropopause are color-coded by altitude, though with different color scales to provide contrast.

tropopause can be considered as directly injected. The visualization suggests that there are not only two but *three* possible pathways into the stratosphere: A large number of particles is directly injected (H1) at the volcano in Eritrea and in the western downwind. The Asian Monsoon circulation (H2) transports fewer particles eastward, which uplift near the East China Sea, as shown in Fig. 8(f). Most of the aerosol in the upper troposphere is carried westwards, taking a north-east turn above the Sahara. Then, another large part of the aerosol seems to enter the stratosphere above North India and Nepal (H3). All but the potential vorticity criterion show fairly good agreement on that. We note that for this result only the global maximum in potential vorticity was used. Considering more information from potential vorticity might create more insight.

The frequency of the events suggests that (H1) and (H3) are probably the main pathways into the stratosphere. The cyclonic circulation in the Asian Summer

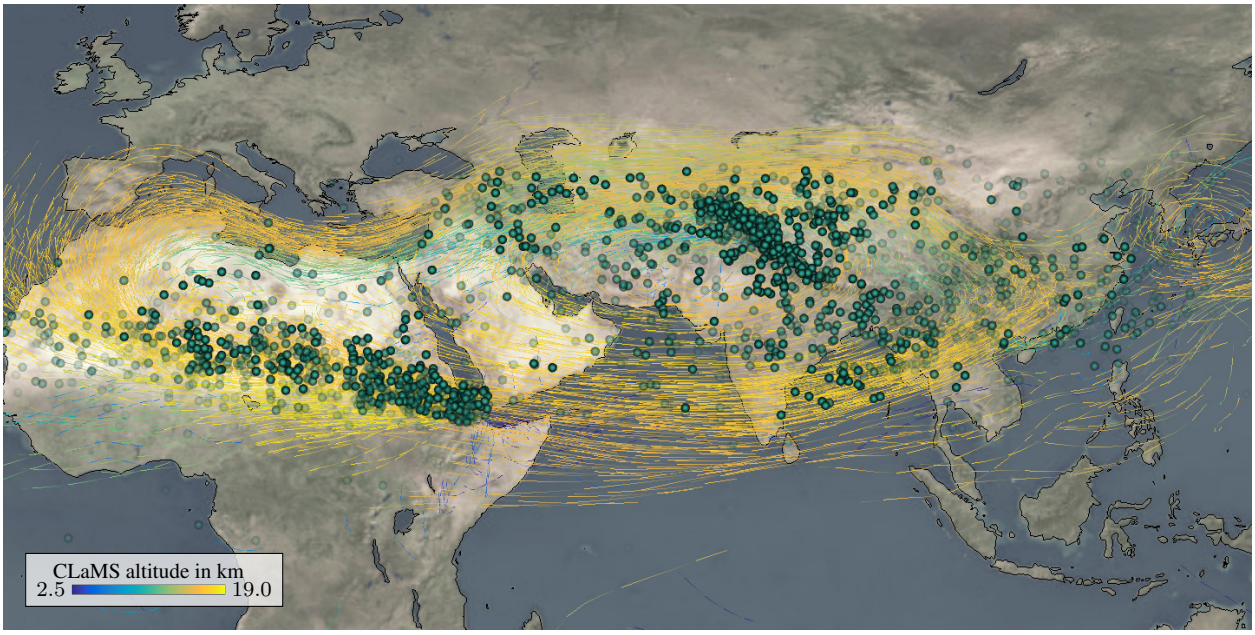

(a) Intersections of CLaMS trajectories with the tropopause.

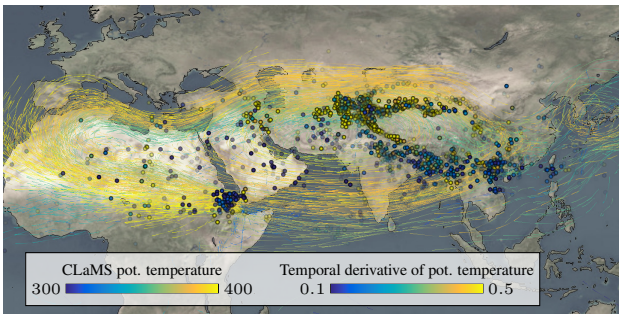

(b) Maximal change in potential temperature.

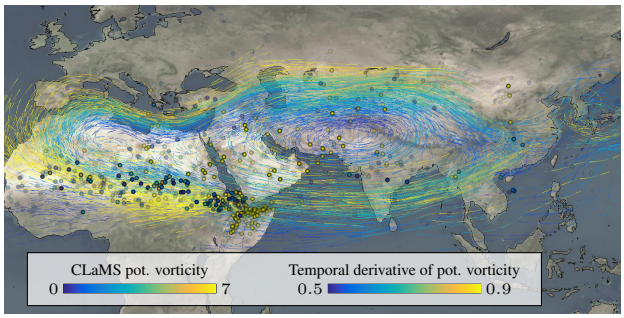

(c) Maximal change in potential vorticity.

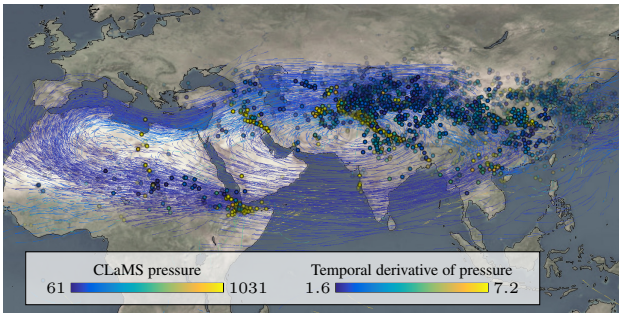

(d) Maximal change in pressure.

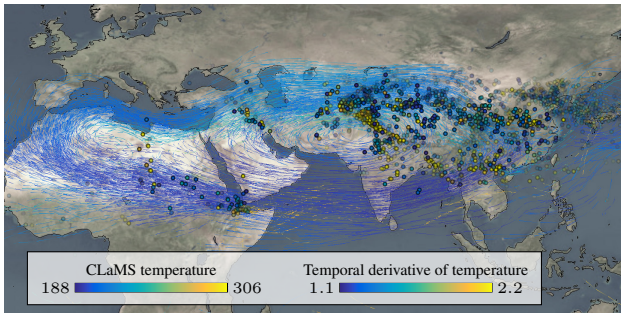

(e) Maximal change in temperature.

Figure 10: A number of different indicators are available to detect vertical transport. In this image, a few of them are shown, plotted as points for the entire time sequence. Points in (a) are intersections of CLaMS trajectories with the lower tropopause geometry layer. The accompanying CLaMS trajectories are color-coded by altitude. A point in (b) to (e) represents the global maximum of the derivative of a certain scalar attribute of a line. Derivatives are with respect to time in Julian hours. The magnitude of the respective derivative is encoded by the point color with the AIRS SO_2 index mapped to opacity ($[0.5, 1] \rightarrow [0, 1]$). The underlying scalar attribute of the line is color-coded on the CLaMS trajectories for reference. CLaMS trajectories are only shown for a time window of 36 hours centered around June 26th in order to reduce clutter. The detections in (d) and (e) over the Eastern Mediterranian Sea show a downward motion.

Monsoon (H2) has a smaller, yet measurable contribution. It should be noted, however, that since actual sulfate aerosol concentrations are not in the data, we mapped the SO_2 index to opacity. Since SO_2 oxidizes over time, the current visualization favors earlier transition events. The quantitative statement of how much sulfate aerosol entered in the three regions should thus be interpreted with care. Nevertheless, the qualitative locations of the three transition regions are very valuable information already.

4 Implementation

Our test system is equipped with an Intel Core i7-2600K CPU with 3.4 GHz, 24 GB RAM and an Nvidia GeForce GTX 560 Ti GPU with 2 GB VRAM. The rendering resolution is at 1440×720 pixels with $4\times$MSAA. During preprocessing, the resampling of the AIRS data took 36 minutes and the mapping of MIPAS detections onto the CLaMS trajectories took 2.3 minutes. At runtime, the visualization reaches interactive frame rates. For instance, the illustrations in Fig. 10 are rendered at 67 frames per second. The rendering of the clouds in Fig. 5 is done at 14 frames per second. The extraction of the cloud scalar fields is implemented on the GPU, using the rasterizer for the rasterization of CLaMS detection values and a compute shader for the distribution of 2D AIRS indices along the altitude axis. As a complete recomputation of the cloud scalar field takes 300 ms it is only performed when a parameter changes.

The visualizations are created in a specifically tailored C++ program that uses Direct3D 11 for rendering. In addition, we used standard tools such as ParaView and ZIB Amira for display of intermediate results throughout the development.

5 Conclusions and Future Work

This paper summarized our contributions to the 2014 IEEE Scientific Visualization Contest, which centered around the assessment of volcanic ash and sulfate aerosol clouds, emitted from three volcanoes in summer 2011. Starting with an overview visualization of the available data, we studied the agreement of MIPAS and AIRS measurements, associated measurements with potential source volcanoes, reconstructed volcanic ash and sulfate clouds, intersected these clouds with exemplary air flight routes, visualized the CLaMS trajectories by opacity optimization, and finally studied indicators for tropopause transitions to locate pathways of Nabro's sulfate aerosol into the stratosphere.

Especially the last study adds new insights to the ongoing discussion on how Nabro's sulfate aerosol entered the stratosphere [BRR*12, FKN*14, VTF*13, BRR*13], as we identified not only two but three locations where it happened. Considering the frequency of transition events in the Nabro case, we argue for a direct injection into stratospheric or upper-tropospheric altitudes as the main pathway into the stratosphere. A cyclonic monsoon circulation seems to be a possible driving mechanism as well, but here, it played a rather minor role.

The original satellite data was partly sparse and included wide measurement gaps. We see much room for further investigations on improved data interpolation, for instance by accounting for atmospheric transport and optional fallbacks for missing data. Also, the association of measurements to the Puyehue-Cordón Caulle and Nabro eruptions relied on CLaMS trajectories only, which are known to become unreliable after more than five days in the troposphere. If sufficient statistics or trajectory ensembles are available they can be reliable for longer time scales. Our cloud reconstruction is based on the assumption that the amount of transported ash corresponds to the density of ash-laden CLaMS trajectories. This might not always be true, as the MIPAS detections that were used to decide whether CLaMS trajectories are ash-laden, give no quantitative measure for the amount of volcanic ash or sulfate aerosol. Integrating the visualization into a live feed of satellite data poses another interesting and worthwhile future challenge.

Acknowledgments

We dearly thank David Feng, Bernd Hentschel, Sabine Grießbach, Lars Hoffmann and Marc von Hobe for their exceptional job of hosting the IEEE Scientific Visualization Contest. We also thank the jury for their hard work of reviewing and rating a wide range of highly competitive entries and are very grateful for their insightful feedback.

References

[BRR*12] BOURASSA A. E., ROBOCK A., RANDEL W. J., DESHLER T., RIEGER L. A., LLOYD N. D., LLEWELLYN E. J. T., DEGENSTEIN D. A.: Large

volcanic aerosol load in the stratosphere linked to Asian monsoon transport. *Science 337*, 6090 (2012), 78–81.

[BRR*13] BOURASSA A. E., ROBOCK A., RANDEL W. J., DESHLER T., RIEGER L. A., LLOYD N. D., LLEWELLYN E. J., DEGENSTEIN D. A.: Response to comments on "Large volcanic aerosol load in the stratosphere linked to Asian monsoon transport". *Science 339*, 6120 (2013), 647.

[CPA*06] CHAHINE M. T., PAGANO T. S., AUMANN H. H., ATLAS R., BARNET C., BLAISDELL J., CHEN L., DIVAKARLA M., ET AL.: AIRS: Improving weather forecasting and providing new data on greenhouse gases. *Bulletin of the American Meteorological Society 87*, 7 (2006), 911–926.

[DUS*11] DEE D. P., UPPALA S. M., SIMMONS A. J., BERRISFORD P., POLI P., KOBAYASHI S., ANDRAE U., ET AL.: The ERA-interim reanalysis: configuration and performance of the data assimilation system. *Quarterly Journal of the Royal Meteorological Society 137*, 656 (2011), 553–597.

[FKN*14] FROMM M., KABLICK G., NEDOLUHA G., CARBONI E., GRAINGER R., CAMPBELL J., LEWIS J.: Correcting the record of volcanic stratospheric aerosol impact: Nabro and Sarychev Peak. *Journal of Geophysical Research: Atmospheres 119*, 17 (2014), 10,343–10,364.

[GHSR14] GRIESSBACH S., HOFFMANN L., SPANG R., RIESE M.: Volcanic ash detection with infrared limb sounding: MIPAS observations and radiative transfer simulations. *Atmospheric Measurement Techniques 7*, 5 (2014), 1487–1507.

[GRT14] GÜNTHER T., RÖSSL C., THEISEL H.: Hierarchical opacity optimization for sets of 3D line fields. *Computer Graphics Forum (Proc. Eurographics) 33*, 2 (2014), 507–516.

[HGM14] HOFFMANN L., GRIESSBACH S., MEYER C. I.: Volcanic emissions from AIRS observations: detection methods, case study, and statistical analysis. *Proc. SPIE 9242, Remote Sensing of Clouds & Atmosphere XIX; Optics in Atmos. Prop. & Adapt. Sys. XVII* (2014), 924214, DOI: 10.1117/12.2066326.

[JB10] JANSEN J., BAVOIL L.: Fourier opacity mapping. In *Proc. Symposium on Interactive 3D Graphics and Games* (2010), pp. 165–172.

[KGG*10] KONOPKA P., GROOSS J.-U., GÜNTHER G., PLOEGER F., POMMRICH R., MÜLLER R., LIVESEY N.: Annual cycle of ozone at and above the tropical tropopause: observations versus simulations with the Chemical Lagrangian Model of the Stratosphere (CLaMS). *Atmospheric Chemistry and Physics 10*, 1 (2010), 121–132.

[KGM*07] KONOPKA P., GÜNTHER G., MÜLLER R., DOS SANTOS F. H. S., SCHILLER C., RAVEGNANI F., ULANOVSKY A., SCHLAGER H., ET AL.: Contribution of mixing to upward transport across the tropical tropopause layer (TTL). *Atmospheric Chemistry and Physics 7*, 12 (2007), 3285–3308.

[MKG*02] MCKENNA D. S., KONOPKA P., GROOSS J.-U., GÜNTHER G., MÜLLER R., SPANG R., OFFERMANN D., ORSOLINI Y.: A new Chemical Lagrangian Model of the Stratosphere (CLaMS) 1. formulation of advection and mixing. *Journal of Geophysical Research: Atmospheres 107*, D16 (2002), DOI: 10.1029/2000JD000114.

[PKM*12] PLOEGER F., KONOPKA P., MÜLLER R., FUEGLISTALER S., SCHMIDT T., MANNERS J. C., GROOSS J.-U., GÜNTHER G., FORSTER P. M., RIESE M.: Horizontal transport affecting trace gas seasonality in the Tropical Tropopause Layer (TTL). *Journal of Geophysical Research: Atmospheres 117*, D09303 (2012), DOI: 10.1029/2011JD017267.

[VTF*13] VERNIER J.-P., THOMASON L. W., FAIRLIE T. D., MINNIS P., PALIKONDA R., BEDKA K. M.: Comment on "Large volcanic aerosol load in the stratosphere linked to Asian monsoon transport". *Science 339*, 6120 (2013), 647.

[ZSH96] ZÖCKLER M., STALLING D., HEGE H.-C.: Interactive visualization of 3D vector fields using illuminated stream lines. In *IEEE Visualization* (1996), pp. 107–113.

Tobias Günther is a PhD student in the Visual Computing Group at University of Magdeburg. His main research interests include scientific visualization, real-time rendering and physically-based light transport. Tobias received a BS in computational visualistics and an MS in computer science, both from University of Magdeburg. Contact him at tobias@isg.cs.ovgu.de.

Maik Schulze is a PhD student in the University of Magdeburg's Visual Computing Group. His research interests include flow visualization, geometry processing and computer graphics. Maik received his diploma in computational visualistics from University of Magdeburg. Contact him at maik@isg.cs.ovgu.de.

Anke Friederici is currently a BS student in computational visualistics at the University of Magdeburg. She is a student assistant in the Visual Computing Group, working in the field of flow visualization. Contact her at anke.friederici@st.ovgu.de.

Holger Theisel is a full professor for Visual Computing at Magdeburg University (Germany) and head of the Visual Computing Group. He received his Ph.D. (1996) and habilitation (2001) degrees from the University of Rostock (Germany), and had research stays at Arizona State University (USA), ICIMAF Havana (Cuba), MPI Informatik Saarbrücken (Germany), and Bielefeld University (Germany). His research interests focus on scientific visualization as well as on geometric design, geometry processing and information visualization. Contact him at theisel@ovgu.de.